

Stable Machine Learning Potentials for Liquid Metals via Dataset Engineering

Alex Tai¹, Jason Ogbebor¹, Rodrigo Freitas^{1†}

¹Department of Materials Science and Engineering, Massachusetts Institute of Technology, Cambridge, MA, USA

Dated: January 9, 2026

Abstract

Liquid metals are central to energy-storage and nuclear technologies, yet quantitative knowledge of their thermophysical properties remains limited. While atomistic simulations offer a route to computing liquid properties directly from atomic motion, the most accurate approach—*ab initio* molecular dynamics (AIMD)—is computationally costly and restricted to short time and length scales. Machine learning interatomic potentials (MLPs) offer AIMD accuracy at far lower cost, but their application to liquids is limited by training datasets that inadequately sample atomic configurations, leading to unphysical force predictions and unstable trajectories. Here we introduce a physically motivated dataset-engineering strategy that constructs liquidlike training data synthetically rather than relying on AIMD configurations. The method exploits the established icosahedral short-range order of metallic liquids—twelvefold, near-close-packed local coordination—and generates “synthetic-liquid” structures by systematic perturbation of crystalline references. MLPs trained on these datasets close the sampling gaps that lead to unphysical predictions, remain numerically stable across temperatures, and reproduce experimental liquid densities, diffusivities, and melting temperatures for multiple elemental metals. The framework links atomic-scale sampling to long-term MD stability and provides a practical route to predictive modeling of liquid-phase thermophysical behavior beyond the limits of direct AIMD.

1. Introduction

Liquid metal properties play a central role across technologies spanning manufacturing, energy storage, and nuclear systems, including additive manufacturing, liquid-metal batteries, and reactor cooling. More specifically, liquid-metal density controls flow, buoyancy, and heat transport, diffusivity governs mass transport and phase-transformation kinetics, and melting temperature defines the operational window for processes involving the solid–liquid phase change. Despite this importance, liquid metal properties remain poorly characterized experimentally. While benchmark density data are available for many pure elemental melts, systematic measurements of alloy melt densities as a function of composition are scarce. Diffusivity is even less well constrained, with reliable experimental data limited or unavailable even for many single-element liquid metals. This scarcity reflects substantial experimental challenges, including extreme temperatures, chemical reactivity with containers, and gravity-driven convection, which often require containerless techniques such as electrostatic or magnetic levitation, microgravity experiments aboard the International Space Station, and access to large-scale facilities such as synchrotrons and neutron sources¹.

An alternative to direct experimentation is to compute liquid-metal properties from atomic motion using molecular dynamics (MD) simulations. In MD, atomic trajectories are obtained by integrating interatomic forces, making the accuracy of the method directly dependent on how these forces are computed. The most accurate MD approach evaluates forces from first-principles electronic-structure calculations at each timestep and is therefore referred to as *ab initio* molecular dynamics (AIMD). However, the high computational cost of these electronic calcu-

lations severely limits the accessible time and length scales, typically to systems containing a few hundred atoms and simulation times of a few picoseconds. Accurately capturing liquid behavior requires substantially larger system sizes and longer trajectories, with tens of thousands of atoms needed to mitigate finite-size effects and hundreds of picoseconds to nanoseconds required for convergence of dynamic properties such as diffusion. These combined spatial and temporal demands render AIMD prohibitively expensive for calculating most liquid properties.

To extend the accessible time and length scales of MD simulations, machine learning interatomic potentials (MLPs) have emerged as computationally efficient alternatives to first-principles calculations. In MLP-based MD, a machine learning model is trained on first-principles data, typically using configurations sampled from AIMD trajectories. Once trained, the model replaces explicit electronic-structure calculations, enabling simulations at substantially larger spatial and temporal scales while retaining an accurate description of interatomic interactions. Despite these advances, two major challenges limit the application of MLPs to liquids. First, MLP-driven MD exhibits instabilities, in which undersampled regions of configuration space lead to unphysical force predictions and unexpected trajectory failure. Second, validation of MLP predictions often relies primarily on test-set errors evaluated on data closely related to the training set.

In this work, we address these two challenges in MLP-based simulation of liquid metals, enabling accurate prediction of key structural, kinetic, and thermodynamic properties in good agreement with experimental data across a range of systems. Our approach is physically motivated by the well-established icosahedral short-range order observed in metallic liquids^{2–5}, in which atoms form densely packed twelvefold coordination environments akin to those in face-centered cubic crystals. By systematically perturb-

[†]Corresponding author (rodrigof@mit.edu).

ing crystalline structures to reproduce this local disorder — while avoiding the use of AIMD to generate training data — we construct synthetic-liquid datasets that capture the essential short-range physics of the liquid state. These datasets enable stable and accurate MD trajectories across temperatures for a range of single-element metal systems, enabling direct validation of structural, dynamical, and thermodynamic liquid properties against experiment.

2. Results

2.1. Limitations of AIMD-based training sets

We select Cu as a representative system for testing MLP training methods and for systematically examining training-set construction and the limitations of AIMD-based approaches. We start by training an Atomic Cluster Expansion (ACE) MLP^{6–9} on liquid Cu AIMD snapshots to illustrate the common problem of MD instability^{10–16}. Figure 1a shows the energy over time for MLP-based MD simulations driven by an MLP trained on snapshots from AIMD runs. For the solid and the liquid near the melting point (1358 K), the simulations are stable. However, at temperatures above the melting point, trajectories become unstable partway through the simulation, effectively crashing the MD simulation. This occurs despite the inclusion in the dataset of structures from AIMD simulations at temperatures up to 2500 K.

The effect of increasing system size on MD stability is shown in fig. 1b, where it can be seen that all simulations using the AIMD-based MLP eventually destabilized. Failure occurs earlier in larger systems, with the product of the number of atoms and the time to failure remaining roughly constant. This behavior can be understood by considering stability in terms of atomic collisions: if any given collision has a small probability of producing an unstable configuration, the overall stability is determined statistically by the expected number of collisions before failure. In an equilibrium system, the total number of collisions scales linearly with both the number of atoms and the simulation time, leading to the observed size- and time-dependent destabilization. Such instability at larger time and length scales poses a challenge for calculating liquid properties of interest with MD, which all require tens of thousands of atoms and long trajectories to achieve proper convergence and statistical averaging.

2.2. Synthetic liquid training sets

To address this instability problem, we developed a “synthetic liquid” (SL) approach for constructing the training dataset for MLPs, illustrated in fig. 1d. This approach is physically motivated by the well-established observation that metallic liquids exhibit pronounced icosahedral short-range order^{2–5}. Diffraction studies and simulations on undercooled Al, Ni, Fe, and other transition metals have shown that atoms in the liquid are not randomly arranged but instead form densely packed cages with twelve nearest neighbors, closely resembling the first coordination shell of a face-centered cubic (fcc) crystal (i.e., a cubocta-

hedron). The fcc cuboctahedron and the icosahedral cluster share nearly identical nearest-neighbor distances, differing only slightly in their angular topology. This geometric kinship provides a natural bridge between crystalline and liquid configurations: perturbing an fcc lattice generates radial and angular correlations characteristic of liquid metals while avoiding the need for costly AIMD sampling. Thus, by systematically introducing random displacements around fcc lattice sites, the SL method mimics the structural statistics of the liquid (i.e., dense local coordination and bond-angle dispersion) within a simple, controllable framework.

In the SL approach, thermal noise is mimicked by randomly displacing atoms from their ideal fcc lattice positions within a spherical volume. The radius of this volume is controlled by a parameter α , which represents the magnitude of the imposed thermal noise and therefore plays a role analogous to temperature. When $\alpha = 1$, the sphere extends halfway to the nearest neighbor, i.e., the maximum possible size without overlapping volumes. The datasets consist of structures with a range of α values, uniformly distributed from 0 up to α_{\max} . Structures are also scaled up in size by applying uniform volumetric (isotropic) strains, with the magnitude uniformly varied from 0% to 5% relative to the ground-state structure. The parameter α can be directly related to the Lindemann melting criterion¹⁷, a well-known rule of thumb for determining when melting occurs:

$$\sqrt{\langle \mu^2 \rangle} \geq \eta d, \quad (1)$$

where μ is the instantaneous displacement of an atom from its lattice position, η is the Lindemann coefficient, and d is the nearest-neighbor distance. The brackets $\langle \cdot \rangle$ denote a thermal average over atomic vibrations, such that $\sqrt{\langle \mu^2 \rangle}$ represents the root-mean-square amplitude of atomic motion at a given temperature. Because α in the SL approach defines a comparable geometric displacement amplitude, it provides a convenient way to mimic the degree of thermal disorder, allowing a direct relationship between α and η to be established:

$$\alpha = \sqrt{\frac{20}{3}}\eta, \quad (2)$$

see Supplementary Information sec. 1 for a derivation of this equation. Copper has $\eta = 0.108$ ¹⁸, which corresponds to $\alpha = 0.279$. Thus, if α can be considered an effective temperature scale, then the “melting point” for SL Cu is $\alpha = 0.279$. We expect that datasets must include structures exceeding this value to capture liquid behavior.

Previous work has shown that MLP instability arises from unphysical model predictions resulting from insufficient coverage of the configuration space, particularly for structures with short interatomic distances^{15,16}. The SL approach provides a more comprehensive exploration of such environments. As shown in fig. 1e, the radial distribution function $g(r)$ of the SL dataset exhibits a longer left tail, indicating inclusion of short-distance interactions rarely observed in AIMD trajectories. Consequently, the SL-based MLP yields stable MD even at high tempera-

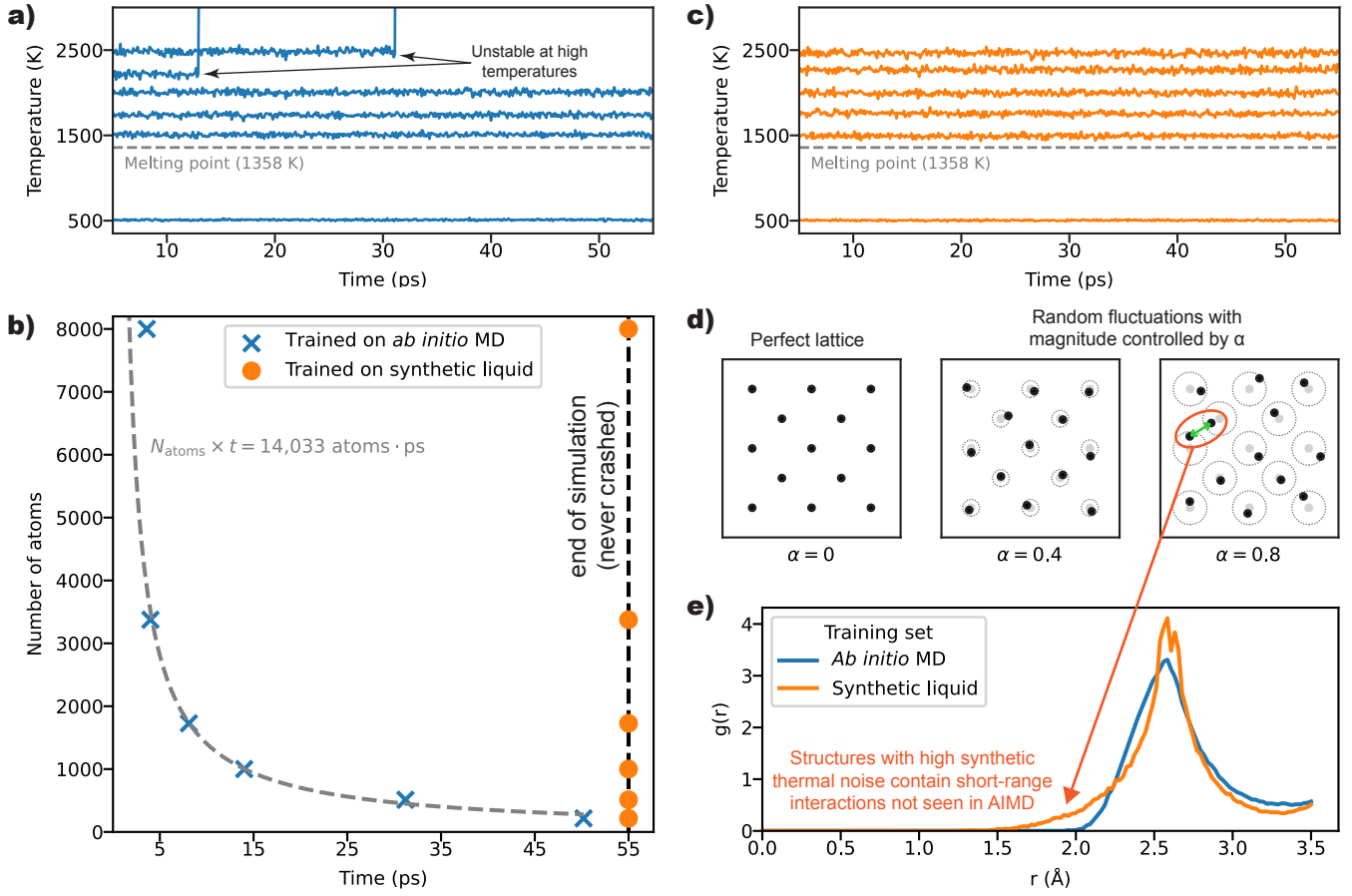


Figure 1: Stabilizing liquid-phase MD with synthetic-liquid training. **a)** Evolution of simulations driven by an MLP trained only on AIMD structures. Simulations destabilize and crash at high temperatures due to unphysical predictions. **b)** Simulation stability as a function of system size and trajectory length at 2500 K. AIMD-trained MLPs destabilize earlier as system size increases, while SL-trained MLPs remain stable for all sizes. **c)** Temperature evolution for synthetic liquid MLPs showing stable trajectories across all temperatures. **d)** Synthetic liquid structures for training are generated by randomly perturbing ideal fcc lattice positions, with the magnitude of perturbation controlled by α . This approach is physically motivated by the icosahedral order in metallic liquids. **e)** Radial distribution functions for the *ab initio* and synthetic liquid training sets. The synthetic liquid set includes short-range interactions not present in AIMD.

tures, as shown in fig. 1b and 1c.

In summary, the SL approach can be viewed as a geometrically grounded method for reproducing the quasi-icosahedral coordination intrinsic to liquid metals through systematic perturbations of a crystalline reference. This dataset-engineering strategy bridges atomic-scale structure and simulation stability, ensuring that key short-range interactions governing liquid behavior are thoroughly represented in the training data.

2.3. Optimizing parameters for synthetic-liquid training set

We now examine how the choice of parameters in the SL approach influences MLP performance, focusing on the magnitude of the thermal noise α . As shown in fig. 1e, short-range interactions are the main distinction between AIMD and SL training sets, making α a key parameter to investigate. To identify its optimal range, we construct multiple datasets with different maximum values α_{\max} . In each dataset, α is varied from 0 (the perfect crystal) up

to α_{\max} . The largest value of α_{\max} considered is 0.8; this limit was chosen because at α values approaching 1.0 the atoms become so close that numerical errors from the treatment of core electrons in density-functional theory (DFT) become significant¹⁹.

To analyze how varying α_{\max} influences the coverage of configuration space, we visualize the local atomic environments sampled by each MLP as a function of α_{\max} . Such environments can be represented using the distances and bond angles among atoms within the MLP cutoff radius r_{cutoff} , as shown in fig. 2a. The radial component of the plots in fig. 2b represents the average bond distance $(r_1 + r_2)/2$, while the angular component represents the bond angle for all interacting triplets of atoms. In the plot for $\alpha_{\max} = 0.2$, the distribution characteristic of the perfect crystal is clearly visible, with significant gaps in coverage remaining. As α_{\max} increases, atomic deviations from ideal lattice positions progressively fill these gaps, and at high α_{\max} values the remaining gaps correspond only to extremely short-distance structures. Analogous plots for

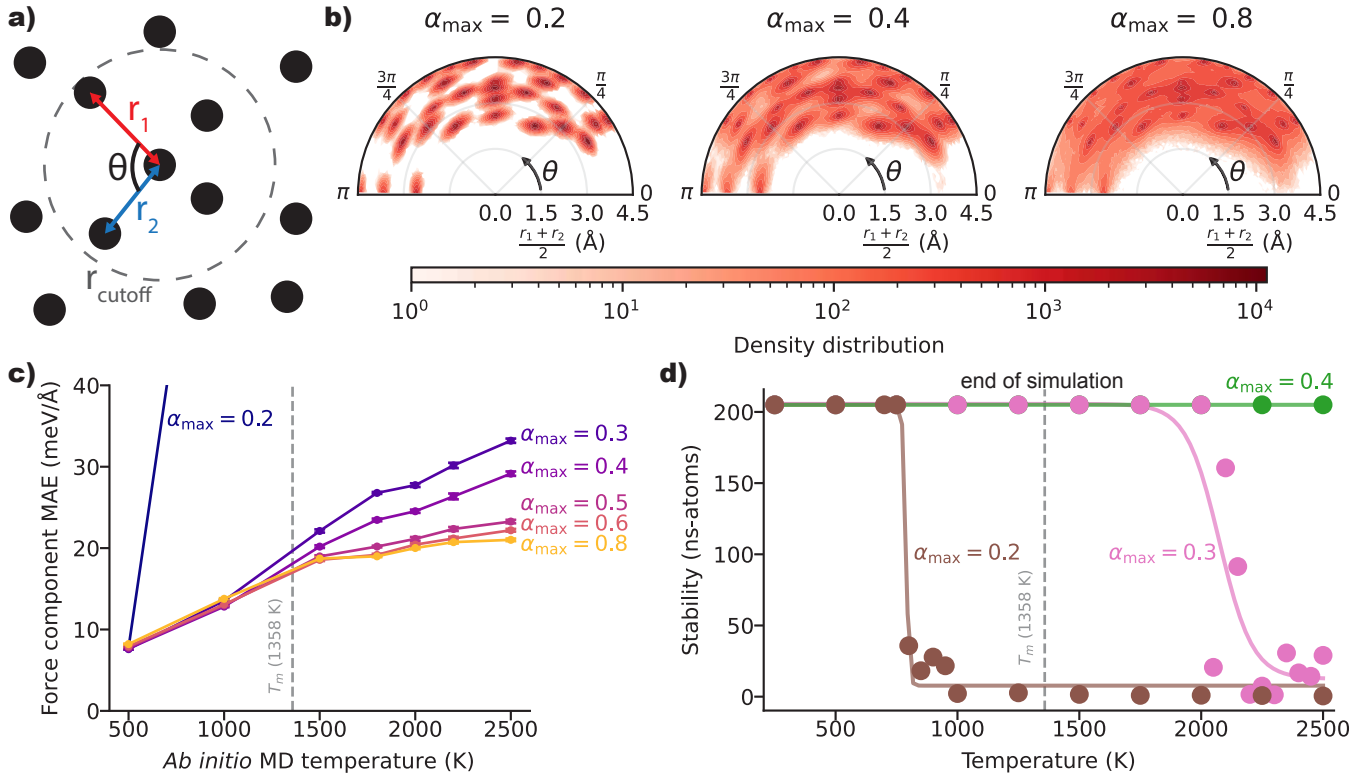


Figure 2: Optimizing α_{max} for synthetic-liquid training. **a)** Schematic of bonds pairs within cutoff radius defining the basis configuration space. **b)** Density distribution of local atomic environments for different α_{max} values. The radial component of the plot represents the average bond distance, while the angular component represents the bond angle. **c)** Mean absolute error of force predictions for MLPs trained on datasets with increasing α_{max} , evaluated on independent AIMD test sets. Error bars represent the standard deviation of the (MAE) obtained from bootstrap resampling 100 times. **d)** Simulation stability (define as the product of simulation time and number of atoms) as function of temperatures for MLPs trained with different α_{max} . Lines are included as a guide to the eye.

AIMD snapshots are presented in Supplementary Information sec. 2, which reveal a similar lack of coverage at short interatomic distances and reinforce the conclusion drawn from fig. 1e: the SL approach systematically samples configurations that are rare or absent in AIMD trajectories, thereby eliminating undersampled regions of configuration space that give rise to MD instability.

To assess the effect of α_{max} on model accuracy, we evaluated the mean absolute prediction error of the force components using independent AIMD test sets. The results are shown in fig. 2c, with the mean absolute errors resolved by AIMD temperature. The analogous plot for energies is provided in the Supplementary Information sec. 5. When $\alpha_{\text{max}} = 0.2$, the MLP exhibits very large errors except at the lowest temperature. Increasing α_{max} improves performance at high temperatures, but the marginal gains diminishing, with $\alpha_{\text{max}} = 0.8$ showing no discernible improvement over $\alpha_{\text{max}} = 0.7$ across the temperature range tested. See Supplementary Information sec. 3 for the effect of α_{max} directly on liquid properties.

As demonstrated in fig. 1a, stability depends on temperature. To explore the nature of the temperature-stability relationship, we quantify stability as the product of simulation time and number of atoms based on the inverse relationship found in fig. 1b. This stability is plotted against

temperature for different α_{max} in fig. 2d. It is clear that for unstable potentials, there is a threshold temperature before which simulations can be reliably completed and beyond which they quickly destabilize. For $\alpha_{\text{max}} = 0.2$ this temperature is around 800 K ($0.59T_m$) and for $\alpha_{\text{max}} = 0.3$ it is around 2000 K ($1.47T_m$). All potentials with higher α_{max} were fully stable at the highest temperature simulated.

2.4. Property benchmarks and exchange-correlation dependence

Having established that SL datasets with sufficiently high α_{max} consistently yield stable MLPs and lower errors, we now turn to the prediction of liquid Cu properties by the SL-trained MLPs and their comparison against available experimental data. Because these MLPs reproduce DFT forces and energies with high fidelity, their comparison with experiment primarily reflects the accuracy of the underlying DFT functionals, and we therefore also compare results obtained from MLPs trained on different exchange-correlation functionals. Figures 3a and 3b show the calculated density and diffusivity of liquid Cu at different temperatures for MLPs trained on DFT data obtained using the PBE³¹ and r2SCAN³² exchange-correlation functionals. PBE is a widely used generalized gradient approximation (GGA) functional, whereas r2SCAN is a more recent

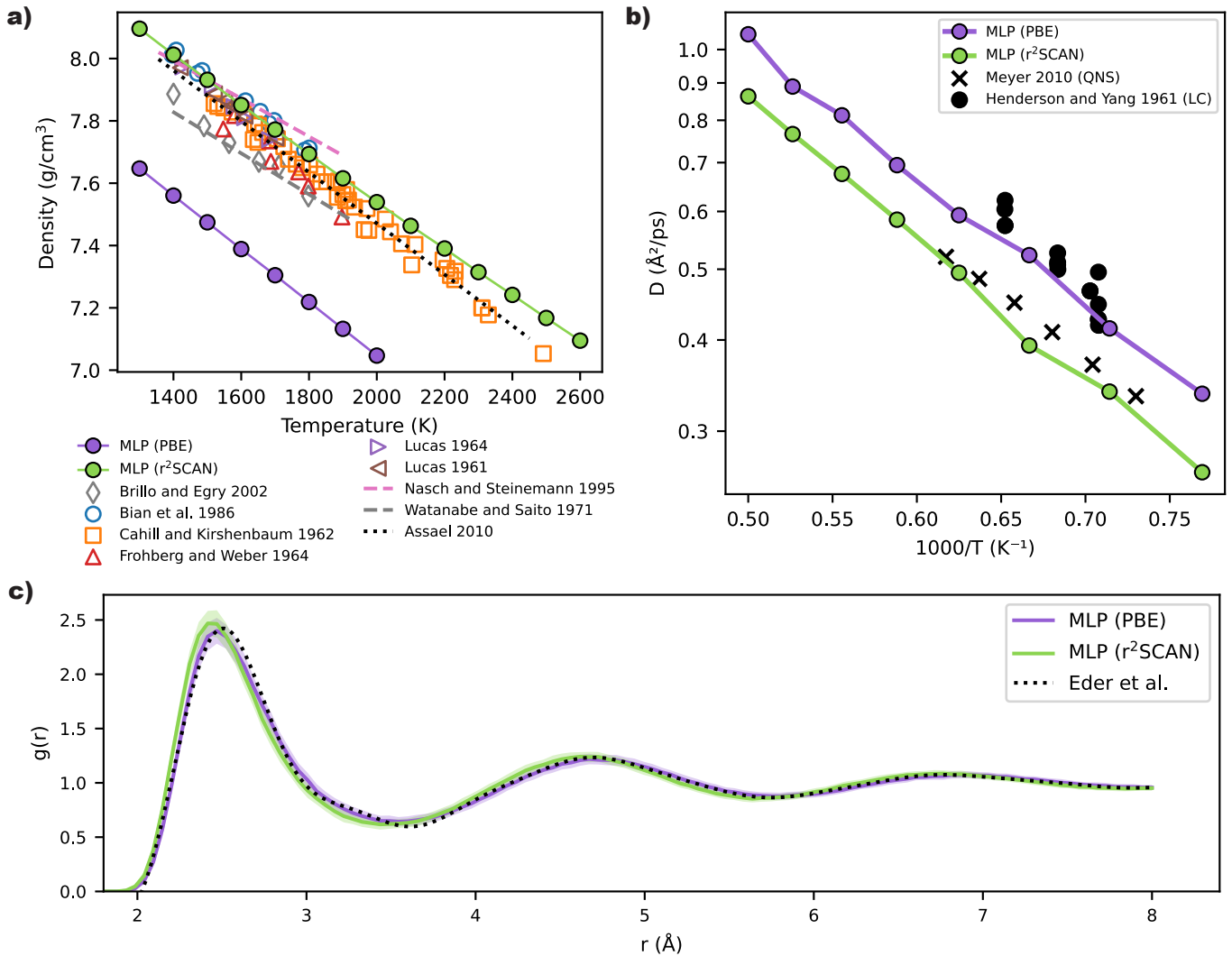


Figure 3: Experimental validation and exchange-correlation functional effects in liquid Cu. a) Temperature dependence of liquid density calculated from MLPs trained with PBE and r²SCAN exchange-correlation functionals, shown alongside experimental measurements^{20–27}, including a meta-analysis by Assael *et al.*²⁷. b) Temperature dependence of diffusivity compared with experimental data from the long capillary method²⁸ (filled circles) and quasi-elastic neutron scattering²⁹ (crosses). c) Radial distribution function for liquid Cu at 1833 K calculated using MLPs, in agreement with experimental results (shaded area is the standard error from the mean)³⁰.

meta-GGA functional that systematically improves the description of bonding and equilibrium structures across a broad range of materials^{33,34}. In our calculations (fig. 3a), the PBE-trained MLP underestimates the liquid density. The considerable scatter in the experimental data shown in the same figure highlights the inherent difficulty of measuring liquid-metal properties and suggests that MLPs trained with r²SCAN may already provide accuracy sufficient for practical applications — a point revisited in sec. 3. The diffusivity results (fig. 3b) show a similar pattern of comparison, although interpretation is less straightforward because the two MLPs align with different experimental datasets. If precedence is given to the quasi-elastic neutron scattering measurements²⁹ — which directly probe atomic-scale diffusion and are typically performed under containerless conditions that eliminate convection and wall interactions

— the r²SCAN functional again provides closer agreement than PBE. Finally, fig. 3c compares the computed and experimental³⁰ radial distribution function (RDF) of liquid Cu at 1833 K, showing close agreement and confirming that the MLPs successfully reproduce the liquid structure.

To assess the generality of the synthetic-liquid training strategy beyond Cu, we trained MLPs for seven additional single-element metals (Al, Co, Mg, Mo, Ni, Ti, and W). For each system, the training dataset was generated following the same procedure established for Cu, with the fcc structure was perturbed using $\alpha_{\max} = 0.6$. This approach ensures consistent sampling of thermally disordered configurations across systems while maintaining comparable coverage of short-range interactions. For systems whose ground state differs from fcc (e.g., bcc for W and hcp for Ti), that structure was also included in the training set to

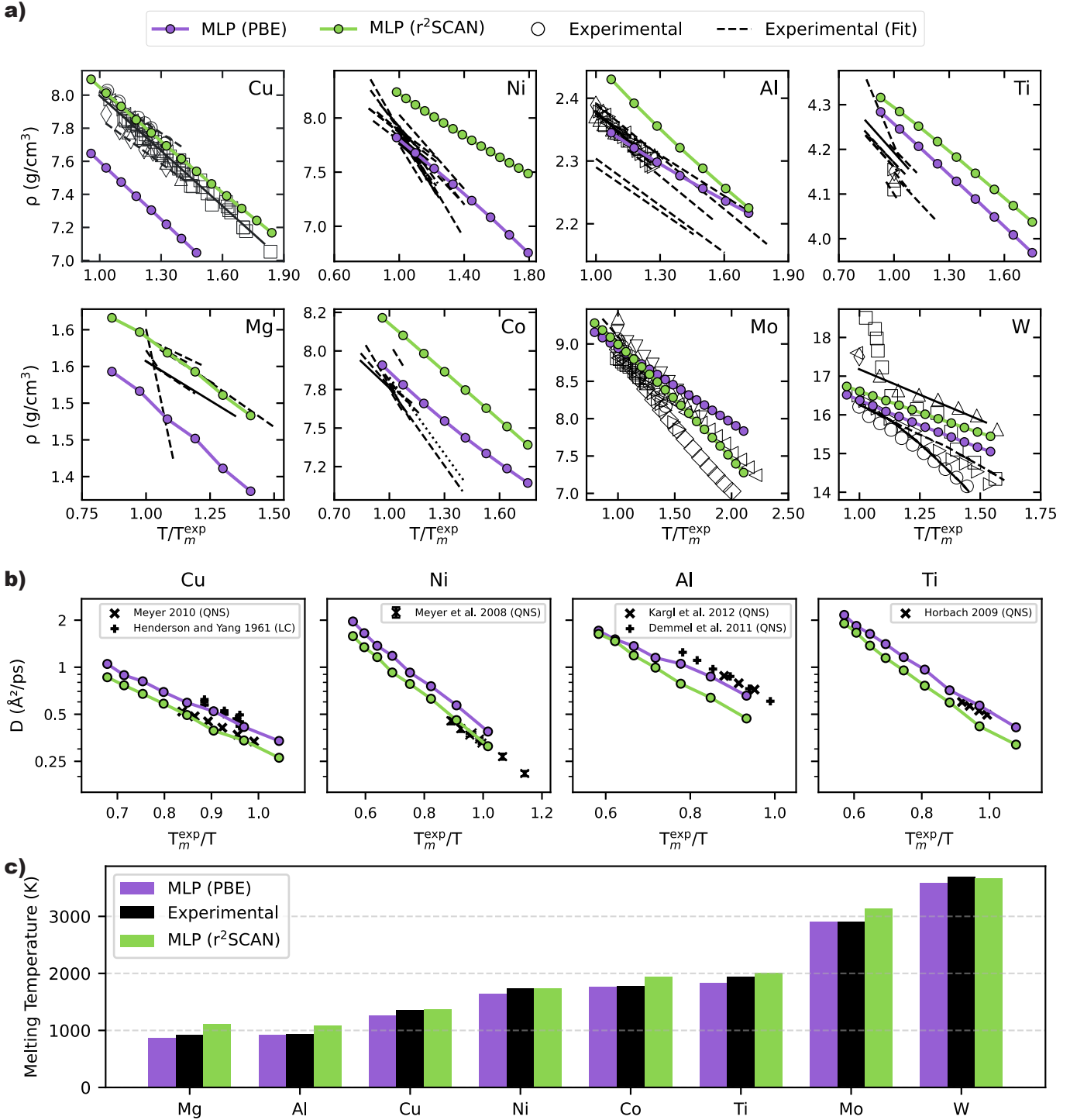


Figure 4: Predicted liquid properties and melting points across elemental metals. **a)** Temperature-dependent liquid density of Al^{25,35–44}, Co^{45–55}, Cu^{20–25,27,52,56}, Mg^{57–64}, Mo^{65–70}, Ni^{20,25,45,48,53,71–90}, Ti^{45,48,69,89,91–98}, and W^{67,69,99–105} predicted by PBE- and r2SCAN-trained MLPs, shown alongside experimental data. Experimental values are plotted in black, with open markers representing individual measurements and dashed lines denoting empirical fits to the experimental datasets. Because detailed labeling would overcrowd the figure, the full list of experimental sources and fit parameters is provided in the Supplementary Information sec. 6. **b)** Diffusivity of Cu^{28,29}, Ni¹⁰⁶, Al^{107,108}, and Ti¹⁰⁹. These four elements are the only systems for which experimental diffusivity data could be found. **c)** Melting points of Mg, Al, Cu, Ni, Co, Ti, Mo and W¹¹⁰. A more detailed analysis of the melting-point errors for each system is provided in the Supplementary Information sec. 8.

provide adequate description of the solid phase. A complete description of all datasets is provided in Supplementary Information sec. 4. Using these MLPs, we computed

the liquid density, diffusivity, and melting point for each metal. These results, together with extensive experimental data collected from the literature, are shown in fig. 4.

To place the comparisons in figs. 4a and 4b in context, it is important to note that experimental data often show substantial scatter for density and diffusivity, which makes it difficult to identify clear systematic deviations between MLP predictions and experiment. Despite this variability, distinct and reproducible trends emerge across exchange-correlation functionals. MLPs trained on r2SCAN calculations predict higher densities and lower diffusivities than those trained on PBE calculations. However, neither functional provides a consistent overall advantage in predictive accuracy of density and diffusivity relative to experiment, suggesting that the optimal choice is system-dependent. For the melting point (fig. 4c), r2SCAN systematically predicts higher values than PBE. But the comparison with experimental data is much clearer: the absolute deviation from experimental measurements for PBE ranges from -117 K to 35 K, corresponding to a relative errors of only -6% to 1% (Supplementary Information sec. 8).

Because of the results discussed above, we sought a simple heuristic for selecting the most suitable exchange-correlation functional based on readily available or easily calculated DFT data. The trends of each functional in predicting the density of the ground-state crystal phase are well established: PBE tends to underbind (overestimating lattice parameters and thus underpredicting density), while r2SCAN slightly overbinds (leading to overpredicted densities)^{33,34}. These behaviors are straightforward to quantify through static DFT calculations of the solid phase. However, analogous trends for liquids are far less well known, since direct DFT simulations of liquid metals are limited by the small system sizes and short timescales accessible to AIMD.

To examine whether these solid-state trends extend to the liquid phase, fig. 5 compares the liquid-density error at the melting point—obtained from MLP predictions—with the solid-density error computed directly from DFT relaxations. The errors were evaluated against experimental data: experimental liquid densities were taken from a single representative study for each element, prioritizing the most recent measurements, while experimental solid densities were corrected to 0 K to enable comparison with DFT results (following the approach by Lejaeghere *et al.*¹¹¹). The correlation observed in fig. 5 indicates that the systematic trends known for the solid phase extend to the liquid phase as well: functionals that overbind or underbind the solid exhibit the same tendency for the liquid. This correspondence implies that the most suitable exchange-correlation functional for liquid-phase simulations can often be inferred directly from the well-known solid-phase behavior.

3. Discussion

MLPs have rapidly expanded the reach of atomistic simulations, but their application to liquids remains limited by difficulties in both dataset generation and model validation. Our results show that these challenges can be systematically addressed by constructing training datasets

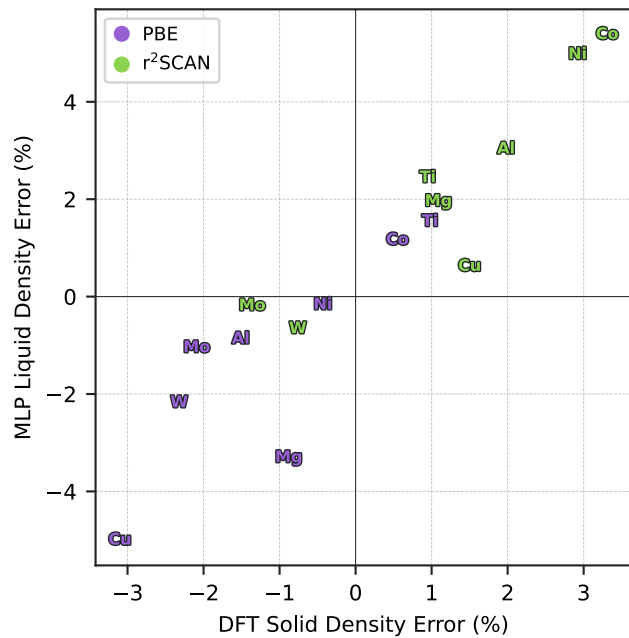


Figure 5: Correlation between solid- and liquid-phase density errors. Comparison of the relative error in liquid density at the melting point (from MLP simulations) with the corresponding solid density error obtained directly from DFT calculations. The strong correlation between the two phases indicates that the well-known binding tendencies of each functional in the solid phase extend to the liquid phase as well.

that intentionally reproduce the statistical features of liquid disorder without relying on AIMD snapshots.

3.1. Training sets and MD stability

The high correlation among structures in AIMD trajectories restricts the sampled configuration space and limits model generality⁶. While AIMD data remain the standard for liquid MLPs^{13,112–118}, they poorly represent short-range atomic encounters that dominate liquid behavior. An obvious alternative—drawing configurations from purely random atomic arrangements—is not practical for metallic liquids, because such structures fail to reflect the known icosahedral short-range order. The SL approach addresses this by constructing training configurations through controlled random perturbations of the fcc crystal lattice (fig. 1d), which systematically include short interatomic distances absent in AIMD (fig. 1e). This construction is not *ad hoc*: it is a compact surrogate for the icosahedral local structure of metallic liquids, ensuring that short-range repulsion and realistic bond-angle variability are both represented in training. Consistent with prior experimental and simulation studies showing quasi-icosahedral short-range order in metallic liquids^{2–5}, the SL-trained MLPs also exhibit a finite population of icosahedrally coordinated atoms in the liquid phase (see Supplementary Information, sec. 9), illustrating that the SL dataset construction emphasizes physically relevant local environments.

This expanded coverage resolves one of the central problems in liquid-phase simulations: MD instability. AIMD-trained MLPs often destabilize at high temperatures due to unphysical predictions in sparsely sampled regions of the potential energy surface (fig. 1a). In contrast, SL-trained MLPs remain stable across all temperatures and system sizes (fig. 1b and 1c). We find that the onset of instability scales with the product of the number of atoms and simulation time (fig. 1b), which reflects the total number of atomic collisions prior to failure. This statistical scaling indicates that stability is controlled by the likelihood of sampling underrepresented configurations during atomic interactions. Increasing α_{\max} expands the explored region of configuration space and eliminates these poorly sampled regions, thereby improving robustness. The resulting MLPs sustain trajectories beyond the length and time scales required for computing liquid properties, establishing a direct connection between dataset engineering and long-term MD stability.

3.2. Rigorous MLP validation

Validation of MLPs has traditionally focused on errors in energies and forces on test sets drawn from the same data pool. However, low test-set error alone does not ensure physical reliability. For example, the model trained with $\alpha_{\max} = 0.3$ has force errors similar to those of larger α_{\max} values at low temperature (fig. 2c) but rapidly destabilizes at high temperature (fig. 2d), illustrating that accurate interpolation does not guarantee robust extrapolation to configurations encountered during MD.

Validation through material properties provides a more stringent and physically meaningful assessment^{15,16}: RDFs reproduce the experimental liquid structure (fig. 3c), and property-level checks on density and diffusivity confirm accuracy over a broad range of conditions (figs. 3a, 3b, 4a, and 4b). Experimental measurements themselves exhibit substantial scatter, often comparable to the full spread between independent studies, which limits the utility of pointwise comparisons between simulations and individual datasets. Within this context, the present results fall consistently within the experimental envelope, indicating that the approach achieves a level of fidelity comparable to the reproducibility of existing experimental measurements and is therefore suitable for practical calculations of liquid-metal properties where experimental data are sparse or inconsistent.

3.3. Exchange–correlation dependence

The accuracy of MLPs is ultimately bounded by the density-functional theory (DFT) functional used to generate the reference data. As shown in fig. 3 and fig. 4, r2SCAN-based MLPs predict higher densities and lower diffusivities than their PBE counterparts, consistent with the overbinding tendency of r2SCAN in solids^{33,34}. Figure 5 confirms that this bias extends systematically from the solid to the liquid phase: functionals that overbind in the solid tend to yield denser liquids, while those that underbind produce lower liquid densities. This correlation

provides a simple heuristic for selecting an appropriate exchange–correlation functional for liquid-phase simulations. While r2SCAN offers improved accuracy for most systems, its poorer description of magnetic metals such as Ni and Co³² indicates that functional performance remains system-dependent.

4. Conclusion

Accurate and stable MLPs for liquid metals can be obtained without AIMD by constructing synthetic-liquid datasets that deliberately sample the relevant configuration space. This framework overcomes a long-standing practical obstacle: naive random placement of atoms produces abundant near-overlaps that neither reflect the known icosahedral short-range order of metallic liquids nor are compatible with standard pseudopotential DFT, which fails when core regions overlap—forcing prior work to rely almost exclusively on costly AIMD snapshots for training. Our method introduces this missing short-range order explicitly, using controlled perturbations of close-packed crystalline environments to reproduce the dense, twelvefold local coordination characteristic of metallic liquids while respecting excluded-volume constraints. By tuning the magnitude of atomic perturbations through α_{\max} captures the short-range interactions that govern stability at high temperatures, enabling MLPs that reproduce experimental liquid densities, diffusivities, and melting points while maintaining numerical stability in large-scale MD simulations that are inaccessible to computationally costly AIMD.

Beyond accuracy, the present framework establishes a transparent and reproducible connection between configurational sampling and long-term MD stability, providing a physically grounded criterion for dataset construction and model validation. Although experimental measurements of liquid-metal properties exhibit substantial scatter across independent studies, the present calculations fall consistently within this experimental envelope. In this regime, agreement at the level of experimental variability represents the strongest validation achievable and underscores the practical value of the approach, particularly where experimental data are sparse, inconsistent, or difficult to obtain.

The predictive ceiling remains set by the underlying DFT functional; however, the correlation between solid- and liquid-phase density errors identified in fig. 5 offers a practical heuristic for functional selection based on readily accessible solid-state calculations. Taken together, this dataset-engineering strategy provides a scalable route to predictive modeling of liquid-phase thermophysical behavior at a consistent level of physical theory, without resorting to AIMD. Because the SL approach is not tied to a specific element or crystal structure, it is readily extendable to multicomponent systems¹¹⁹, where experimental data on liquid properties are virtually nonexistent. Its application to alloys enables systematic evaluation of composition-dependent thermophysical behavior, thereby advancing the computational design of materials and processes governed

by liquid-metal properties.

5. Methods

5.1. Density-functional theory

All density-functional theory (DFT) calculations were performed using the Vienna *ab initio* Simulation Package (VASP)¹²⁰ version 6.2.1. The projector augmented-wave (PAW) method was employed with pseudopotentials from the `potpaw.64` library, and the electronic exchange-correlation energy was described using the generalized-gradient approximation (GGA) in the Perdew–Burke–Ernzerhof (PBE) formulation^{120–124} and the meta-GGA in the r2SCAN formulation³².

Pseudopotential	Energy cutoff (eV)	Minimum distance (Å)
Al	400	45
Cu_pv	550	40
Cr_pv	400	45
Mg_pv	500	45
W_sv	350	45
Mo_pv	400	55
Co	400	30
Ni_pv	500	40

Table 1: Converged DFT parameters for each element to within 1 meV/atom. Energy cutoffs and minimum distances are similar to the recommended values by VASP^{120,125} and the KpLib database^{126,127}, respectively.

Reciprocal-space integrations were performed using k -point grids generated with the KpLib algorithm^{126,127}. The minimum allowed distance between lattice points in the real-space superlattice was set to the converged values listed in table 1. Γ -centered grids were excluded in all cases. Electronic occupancies were evaluated using Methfessel–Paxton smearing with a width of 0.2 eV. Spin polarization was enabled only for calculations involving Co and Ni. Static self-consistent field (SCF) cycles were converged to a total energy tolerance of 10^{-6} eV.

5.2. Ab initio molecular dynamics

AIMD simulations were performed for elemental Cu using a 108-atom face-centered cubic (fcc) supercell. All simulations were carried out in the isothermal–isobaric (NPT) ensemble at temperatures ranging from 100 K to 2500 K and zero external pressure. Temperature and pressure were controlled using a Langevin thermostat and Langevin barostat, each with a friction coefficient of 10 ps^{-1} applied to both atomic and lattice degrees of freedom. Ionic motion was integrated with a timestep of 3 fs, and each trajectory was propagated for at least 9 ps to ensure adequate equilibration at every temperature.

Electronic structure evaluations during AIMD employed only the Γ point for Brillouin-zone sampling. Methfessel–Paxton smearing with a width of $\sigma = 0.1$ eV was used to determine electronic occupancies.

5.3. Training set composition

Training datasets for the Cu SL MLPs consisted of 50 static DFT calculations on 108-atom supercells derived from the ground-state fcc crystal structure. Atomic positions were randomly displaced from their lattice sites within a spherical volume centered on the ideal lattice positions. The choice to perturb close-packed crystalline environments reflects established evidence that liquid metals organize into locally icosahedral, twelve-coordinated cages at nearly crystalline nearest-neighbor distances^{3,4}. The displacement of each atom was parametrized in spherical coordinates as

$$\phi = 2\pi x_\phi \quad (3)$$

$$\theta = \cos^{-1}(-1 + 2x_\theta) \quad (4)$$

$$R = \alpha d \sqrt[3]{x_R} \quad (5)$$

where x is a random number uniformly distributed in the interval $[0,1]$, α is a tunable displacement amplitude, and d is half the nearest-neighbor distance in the ground-state crystal. To avoid overlapping atomic positions, α should not exceed 1.

Structures were generated with α values uniformly distributed from 0 up to α_{\max} , and with isotropic lattice scaling applied up to 5% relative to the equilibrium lattice parameter. Following the optimization of α parameters, all datasets employed a α_{\max} of 0.6.

We follow a similar procedure for generating SL datasets for Al, Cr, Mg, W, Mo, Co, and Ni. For systems whose ground state differs from fcc (e.g., bcc for W and hcp for Ti), that structure was also included in the training set to provide adequate description of the solid phase. Each dataset consists of 50 total structures, with 48 (fcc) or 52 (bcc, hcp) atoms per structure. A complete description of all datasets is provided in Supplementary Information sec. 4.

The interatomic MLP trained on AIMD-based data for Cu employed configurations extracted from the AIMD trajectories described in sec. 5.2. These AIMD simulations spanned temperatures from 100 K to 2500 K, covering both solid and liquid phases. Snapshots were sampled at intervals of at least 450 fs, excluding the initial 1.5 ps of equilibration. Each configuration was subsequently recomputed with static DFT calculations using the same computational parameters described in sec. 5.1, and the resulting data were aggregated into the AIMD-based training set.

5.4. MLP training

ACE potentials were fit with pacemaker^{6,7,9,128}. The radial cutoff was set to 4.75 Å for all potentials. The relative weighting factor between energy and force terms in the loss function, κ , was set to 0.1. A body-order ladder scheme was employed, incrementally increasing the number of basis functions by steps of 25. For each ladder step, the training was performed for up to 1400 iterations. The final MLP contained 224 basis functions and a total of 808 trainable parameters. To ensure physical behavior at very short interatomic distances, a Ziegler–Biersack–Littmark

(ZBL) core repulsion potential was applied to all atom pairs at separations shorter than the minimum bond distance present in the corresponding dataset¹²⁹.

5.5. Molecular dynamics

Molecular dynamics (MD) simulations with the MLPs were performed using the Large-scale Atomic/Molecular Massively Parallel Simulator (LAMMPS)¹³⁰ to evaluate structural and transport properties, as well as to assess model stability across system sizes and temperatures. A table with summary of all computed properties is available in Supplementary Information sec. 7.

For the calculation of the RDF in figs. 1e and 3c, simulations were initialized from 108 randomly positioned, non-overlapping atoms. Each trajectory was run for 200 ps in the isothermal-isobaric (NPT) ensemble using a Nosé-Hoover thermostat relaxation time of 1 ps and Nosé-Hoover barostat relaxation time of 10 ps¹³¹⁻¹³⁴. The initial 5 ps of equilibration were excluded from the RDF analysis.

To evaluate the MD stability of MLPs in figs. 1a-c and 2d, simulations were initialized from random atomic positions and equilibrated for 5 ps in the NPT ensemble (thermostat 0.1 ps, barostat 1 ps) at 2500 K. The systems were then evolved for 50 ps in the microcanonical (NVE) ensemble. A trajectory was classified as destabilized if any atoms were lost or if the instantaneous temperature exceeded 4000 K.

For density calculations in figs. 3a and 4a, systems containing 10,000 atoms were initialized from random positions and equilibrated for 60 ps in the NPT ensemble with thermostat and barostat relaxation times of 1 ps and 10 ps, respectively. The density was obtained by averaging the simulation cell volume over the final 40 ps of the trajectory.

For diffusivity calculations (figs. 3b and 4b), systems of 10,000 atoms were first equilibrated for 20 ps in the canonical (NVT) ensemble using a thermostat relaxation time of 1 ps, with the simulation volume fixed to that obtained from the corresponding density calculation. The systems were then propagated for 40 ps in the NVE ensemble, and the mean-squared displacement (MSD) of the atoms was tracked over time. The self-diffusion coefficient D was computed from the linear regime of the MSD curve as

$$D = \frac{\langle |\mathbf{r}(t) - \mathbf{r}(0)|^2 \rangle}{6t} \quad (6)$$

where t is time and \mathbf{r} is distance from the initial position such that the numerator of the right hand side is the MSD. The temperature dependence of diffusivity fitted to the Arrhenius relation:

$$D = D_0 \exp\left(\frac{-\Delta E}{k_B T}\right), \quad (7)$$

where D_0 is the pre-exponential factor, ΔE is the activation energy, k_B is the Boltzmann constant, and T is the temperature.

5.6. Melting point calculation

The melting temperatures of the MLPs (fig. 4c) was determined by calculating the free energies of the solid and liquid phases across their stable and metastable temperature ranges and identifying the temperature at which these phases are in thermodynamic equilibrium. To calculate the free-energies, we employed the non-equilibrium thermodynamic integration (NETI) approach¹³⁵⁻¹³⁷, using LAMMPS to perform the necessary simulations. We first computed the free energies of both phases at the extremes of their selected temperature ranges, followed by the temperature dependence computed via the reversible scaling method¹³⁸. All simulations used a timestep of 1 fs.

For solid phases, we used the Frenkel-Ladd method^{137,139}, in which we compute the free-energy difference between the MLP of interest and an idealized Einstein crystal. The spring constant and equilibrium volume were determined from simulations in the isothermal-isobaric ensemble, which ran for a total of 50,000 timesteps using systems of 2,000 atoms for bcc and 2,048 atoms for fcc. The subsequent constant-volume NETI simulation ran for 10,000 timesteps for equilibration and 50,000 timesteps for the non-equilibrium switching procedure with systems of 11,664 atoms for bcc and 10,976 atoms for fcc. The reversible scaling simulations used the same number of atoms as the Frenkel-Ladd simulations, and the same timing parameters for equilibration and switching. Previous work¹³⁷ has demonstrated the effect of system size and timing parameters on the precision of these methods, and the selected sizes and duration are sufficient for a well-converged result.

For liquid phases, we used the Uhlenbeck-Ford (UF) model¹⁴⁰ as the reference state in our NETI simulations¹⁴¹, for which the absolute free energy can be computed exactly with the help of pre-calculated virial coefficients for select values of the interaction parameters¹⁴². Simulations in the isothermal-isobaric ensemble followed the same details as described for the solid phases. For the subsequent NETI simulations, the parameters of the UF model were set to $p = 75$ and $\sigma = 1.5$ for all MLPs. We found that these parameters are a good choice for all liquid metals in general. An increase in p and/or σ did not result in any significant improvement in the precision or efficiency of the NETI method. Timing parameters for the reversible scaling simulations are the same as the ones used for the solid phases, and system sizes were also chosen to exactly match the corresponding solid phase.

6. Data and code availability

The interatomic MLPs described in this work, along with the DFT calculations used to fit them, will be deposited to the ColabFit Exchange via the OpenKIM framework. The models will be assigned permanent API-identifiers in the OpenKIM repository and made publicly accessible via ColabFit. Any additional scripts, input files, or analysis code associated with the project can be shared through a GitHub repository upon request.

7. Author contributions

J.O. performed all melting-point calculations. A.T. carried out all the other simulations and all subsequent data analysis. All authors contributed to the interpretation of the results, drafted the manuscript, and approved the final version of the paper.

8. Acknowledgments

This work was supported by the Portuguese Foundation for International Cooperation in Science, Technology and Higher Education in the MIT–Portugal Program. The authors acknowledge the MIT Office of Research Computing and Data for providing high performance computing resources that have contributed to the research results reported within this paper.

9. Competing interests

The authors declare no competing interests.

References

- [1] Haruka Tamaru, Chihiro Koyama, Hideki Saruwatari, Yasuhiro Nakamura, Takehiko Ishikawa, and Tetsuya Takada, “Status of the electrostatic levitation furnace (ELF) in the ISS-KIBO”, *Microgravity Science and Technology* (2018), doi: [10.1007/s12217-018-9631-8](https://doi.org/10.1007/s12217-018-9631-8).
- [2] Frederick Charles Frank, “Supercooling of liquids”, *Proceedings of the Royal Society of London. Series A. Mathematical and Physical Sciences* (1952), doi: [10.1098/rspa.1952.0194](https://doi.org/10.1098/rspa.1952.0194).
- [3] T Schenk, D Holland-Moritz, V Simonet, R Bellissent, and DM Herlach, “Icosahedral short-range order in deeply undercooled metallic melts”, *Physical review letters* (2002), doi: [10.1103/PhysRevLett.89.075507](https://doi.org/10.1103/PhysRevLett.89.075507).
- [4] KF Kelton, GW Lee, A Kt Gangopadhyay, RW Hyers, TJ Rathz, JR Rogers, ;? format?; MB Robinson, and DS Robinson, “First X-Ray Scattering Studies on Electrostatically Levitated Metallic Liquids:;? format?; Demonstrated Influence of Local Icosahedral Order on the Nucleation Barrier”, *Physical Review Letters* (2003), doi: [10.1103/PhysRevLett.90.195504](https://doi.org/10.1103/PhysRevLett.90.195504).
- [5] GW Lee, AK Gangopadhyay, KF Kelton, RW Hyers, TJ Rathz, JR Rogers, and DS Robinson, “Difference in icosahedral short-range order in early and late transition metal liquids”, *Physical review letters* (2004), doi: [10.1103/PhysRevLett.93.037802](https://doi.org/10.1103/PhysRevLett.93.037802).
- [6] Ralf Drautz, “Atomic cluster expansion for accurate and transferable interatomic potentials”, *Physical Review B* (2019), Publisher: American Physical Society, doi: [10.1103/PhysRevB.99.014104](https://doi.org/10.1103/PhysRevB.99.014104).
- [7] Yury Lysogorskiy, Cas van der Oord, Anton Bochkarev, Sarath Menon, Matteo Rinaldi, Thomas Hammerschmidt, Matous Mrovec, Aidan Thompson, Gábor Csányi, Christoph Ortner, and Ralf Drautz, “Performant implementation of the atomic cluster expansion (PACE) and application to copper and silicon”, en, *npj Computational Materials* (2021), Number: 1 Publisher: Nature Publishing Group, issn: 2057-3960, doi: [10.1038/s41524-021-00559-9](https://doi.org/10.1038/s41524-021-00559-9).
- [8] Anton Bochkarev, Yury Lysogorskiy, Sarath Menon, Mi-naam Qamar, Matous Mrovec, and Ralf Drautz, “Efficient parametrization of the atomic cluster expansion”, *Physical Review Materials* (2022), doi: [10.1103/PhysRevMaterials.6.013804](https://doi.org/10.1103/PhysRevMaterials.6.013804).
- [9] Yury Lysogorskiy, Anton Bochkarev, Matous Mrovec, and Ralf Drautz, “Active learning strategies for atomic cluster expansion models”, *Physical Review Materials* (2023), doi: [10.1103/PhysRevMaterials.7.043801](https://doi.org/10.1103/PhysRevMaterials.7.043801).
- [10] Xiang Fu, Zhenghao Wu, Wujie Wang, Tian Xie, Sinan Keten, Rafael Gomez-Bombarelli, and Tommi Jaakkola, *Forces are not Enough: Benchmark and Critical Evaluation for Machine Learning Force Fields with Molecular Simulations*, arXiv:2210.07237 [physics], 2023, doi: [10.48550/arXiv.2210.07237](https://doi.org/10.48550/arXiv.2210.07237).
- [11] Sina Stocker, Johannes Gasteiger, Florian Becker, Stephan Günemann, and Johannes T. Margraf, “How robust are modern graph neural network potentials in long and hot molecular dynamics simulations?”, en, *Machine Learning: Science and Technology* (2022), Publisher: IOP Publishing, issn: 2632-2153, doi: [10.1088/2632-2153/ac9955](https://doi.org/10.1088/2632-2153/ac9955).
- [12] Akshay Krishna Ammothum Kandy, Kevin Rossi, Alexis Raulin-Foissac, Gaétan Laurens, and Julien Lam, “Comparing transferability in neural network approaches and linear models for machine-learning interaction potentials”, *Physical Review B* (2023), Publisher: American Physical Society, doi: [10.1103/PhysRevB.107.174106](https://doi.org/10.1103/PhysRevB.107.174106).
- [13] Márcio S. Gomes-Filho, Alberto Torres, Alexandre Reily Rocha, and Luana S. Pedroza, “Size and Quality of Quantum Mechanical Data Set for Training Neural Network Force Fields for Liquid Water”, *The Journal of Physical Chemistry B* (2023), Publisher: American Chemical Society, issn: 1520-6106, doi: [10.1021/acs.jpcb.2c09059](https://doi.org/10.1021/acs.jpcb.2c09059).
- [14] Dávid Péter Kovács, Cas van der Oord, Jiri Kucera, Alice E. A. Allen, Daniel J. Cole, Christoph Ortner, and Gábor Csányi, “Linear Atomic Cluster Expansion Force Fields for Organic Molecules: Beyond RMSE”, *Journal of Chemical Theory and Computation* (2021), Publisher: American Chemical Society, issn: 1549-9618, doi: [10.1021/acs.jctc.1c00647](https://doi.org/10.1021/acs.jctc.1c00647).
- [15] Yifan Cao, Killian Sheriff, and Rodrigo Freitas, “Capturing short-range order in high-entropy alloys with machine learning potentials”, *npj Computational Materials* (2025), doi: [10.1038/s41524-025-01722-2](https://doi.org/10.1038/s41524-025-01722-2).
- [16] Killian Sheriff, Yifan Cao, Tess Smidt, and Rodrigo Freitas, “Quantifying chemical short-range order in metallic alloys”, *Proceedings of the National Academy of Sciences* (2024), doi: [10.1073/pnas.2322962121](https://doi.org/10.1073/pnas.2322962121).
- [17] FA Lindemann, “The calculation of molecular vibration frequencies Phys”, *Physikalische Zeitschrift* (1910).
- [18] Melvin M Vopson, Nassina Rogers, and Ian Hepburn, “The generalized Lindemann melting coefficient”, *Solid State Communications* (2020), doi: [10.1016/j.ssc.2020.113977](https://doi.org/10.1016/j.ssc.2020.113977).
- [19] Leonid Burakovskiy, Darby Jon Luscher, Dean Preston, Sky Sjue, and Diane Vaughan, “Generalization of the Unified Analytic Melt-Shear Model to Multi-Phase Materials: Molybdenum as an Example”, *Crystals* (2019), issn: 2073-4352, doi: [10.3390/crust9020086](https://doi.org/10.3390/crust9020086).
- [20] J. Brillo and I. Egry, “Density Determination of Liquid Copper, Nickel, and Their Alloys”, en, *International Journal of Thermophysics* (2003), issn: 1572-9567, doi: [10.1023/A:1025021521945](https://doi.org/10.1023/A:1025021521945).
- [21] JA Cahill and AD Kirshenbaum, “The Density of liquid copper from its melting point (1356 k.) to 2500 k. and an estimate of its critical constants”, *The Journal of Physical Chemistry* (1962), doi: [10.1021/j100812a027](https://doi.org/10.1021/j100812a027).

[22] Martin G Frohberg and Rudolf Weber, "Dichtemesungen an Eisen-Kobalt-und Eisen-Kupfer-Legierungen", *Archiv für das Eisenhüttenwesen* (1964), DOI: [10.1002/srin.196402388](https://doi.org/10.1002/srin.196402388).

[23] BIAN Maoshu, MA Luming, and WANG Jingtang, "A new method for measuring density of high temperature melt", *Acta Metall Sin* (1986).

[24] LD Lucas, "Densite de l'argent, du cuivre, du palladium et du platine à l'état liquide", *COMPTE RENDUS HEBDOMADAIRE DES SEANCES DE L'ACADEMIE DES SCIENCES* (1961).

[25] P. M. Nasch and S. G. Steinemann, "Density and Thermal Expansion of Molten Manganese, Iron, Nickel, Copper, Aluminum and Tin by Means of the Gamma-Ray Attenuation Technique", en, *Physics and Chemistry of Liquids* (1995), ISSN: 0031-9104, 1029-0451, DOI: [10.1080/00319109508030263](https://doi.org/10.1080/00319109508030263).

[26] S Watanabe and T Saito, "DENSITIES OF BINARY CU BASED ALLOYS IN THE LIQUID STATE", *J JAPAN INST METALS* (1971).

[27] Marc J Assael, Agni E Kalyva, Konstantinos D Antoniadis, R Michael Banish, Ivan Egry, Jiangtao Wu, and William A Wakeham, "Reference Data for the Density and Viscosity of Liquid Copper and Liquid Tin", en, *J. Phys. Chem. Ref. Data* (2010), DOI: [10.1063/1.3467496](https://doi.org/10.1063/1.3467496).

[28] J Henderson and Ling Yang, "Self-diffusion of copper in molten copper", *TRANS METALL SOC AIME* (1961).

[29] A Meyer, "Self-diffusion in liquid copper as seen by quasielastic neutron scattering", *Physical Review B—Condensed Matter and Materials Physics* (2010), DOI: [10.1103/physrevb.81.012102](https://doi.org/10.1103/physrevb.81.012102).

[30] OJ Eder, B Kunsch, M Suda, E Erdpresser, and H Stiller, "The structure factor of liquid copper at 1393K and 1833K", *Journal of Physics F: Metal Physics* (1980), DOI: [10.1088/0305-4608/10/2/008](https://doi.org/10.1088/0305-4608/10/2/008).

[31] John P Perdew, Kieron Burke, and Matthias Ernzerhof, "Generalized gradient approximation made simple", *Physical review letters* (1996), DOI: [10.1103/physrevlett.77.3865](https://doi.org/10.1103/physrevlett.77.3865).

[32] James W. Furness, Aaron D. Kaplan, Jinliang Ning, John P. Perdew, and Jianwei Sun, "Accurate and Numerically Efficient r2SCAN Meta-Generalized Gradient Approximation", *The Journal of Physical Chemistry Letters* (2020), Publisher: American Chemical Society, DOI: [10.1021/acs.jpclett.0c02405](https://doi.org/10.1021/acs.jpclett.0c02405).

[33] Fabien Tran, Julia Stelzl, and Peter Blaha, "Rungs 1 to 4 of DFT Jacob's ladder: Extensive test on the lattice constant, bulk modulus, and cohesive energy of solids", *The Journal of chemical physics* (2016), DOI: [10.1063/1.4948636](https://doi.org/10.1063/1.4948636).

[34] Guo-Xu Zhang, Anthony M Reilly, Alexandre Tkatchenko, and Matthias Scheffler, "Performance of various density-functional approximations for cohesive properties of 64 bulk solids", *New Journal of Physics* (2018), DOI: [10.1088/1367-2630/aac7f0](https://doi.org/10.1088/1367-2630/aac7f0).

[35] Marc J. Assael, Konstantinos Kakosimos, R. Michael Banish, Jürgen Brillo, Ivan Egry, Robert Brooks, Peter N. Quested, Kenneth C. Mills, Akira Nagashima, Yuzuru Sato, and William A. Wakeham, "Reference Data for the Density and Viscosity of Liquid Aluminum and Liquid Iron", en, *Journal of Physical and Chemical Reference Data* (2006), ISSN: 0047-2689, 1529-7845, DOI: [10.1063/1.2149380](https://doi.org/10.1063/1.2149380).

[36] Patrick M Smith, John W Elmer, and Gilbert F Gallegos, "Measurement of the density of liquid aluminum alloys by an x-ray attenuation technique", en, *Scripta Materialia* (1999), ISSN: 13596462, DOI: [10.1016/S1359-6462\(99\)00043-3](https://doi.org/10.1016/S1359-6462(99)00043-3).

[37] S. P. Yatsenko, V. I. Kononenko, and A. L. Suhman, *High Temperature* (1972).

[38] E. S. Levin, G. D. Ayushina, and P. V. Geld, *High Temperature* (1968).

[39] W.J. Coy and R.S. Mateer, *Transactions of the American Society for Metals* (1955).

[40] E. Gebhardt, M. Becker, and S. Dorner, *Aluminium* (1955).

[41] Matthias Leitner, Thomas Leitner, Alexander Schmon, Kirmanj Aziz, and Gernot Pottlacher, "Thermophysical Properties of Liquid Aluminum", en, *Metallurgical and Materials Transactions A* (2017), ISSN: 1543-1940, DOI: [10.1007/s11661-017-4053-6](https://doi.org/10.1007/s11661-017-4053-6).

[42] H. L. Peng, Th. Voigtmann, G. Kolland, H. Kobatake, and J. Brillo, "Structural and dynamical properties of liquid Al-Au alloys", en, *Physical Review B* (2015), ISSN: 1098-0121, 1550-235X, DOI: [10.1103/PhysRevB.92.184201](https://doi.org/10.1103/PhysRevB.92.184201).

[43] W.D. Drotning, *Thermal expansion and density measurements of molten and solid materials at high temperatures by the gamma attenuation technique*, en, tech. rep., 1979, DOI: [10.2172/6007362](https://doi.org/10.2172/6007362).

[44] Julianna Schmitz, Bengt Hallstedt, Jürgen Brillo, Ivan Egry, and Michael Schick, "Density and thermal expansion of liquid Al-Si alloys", en, *Journal of Materials Science* (2012), ISSN: 0022-2461, 1573-4803, DOI: [10.1007/s10853-011-6219-8](https://doi.org/10.1007/s10853-011-6219-8).

[45] Lei Wang, Yong Chan Cho, Yun-Hee Lee, John Jonghyun Lee, and Geun Woo Lee, "Density measurement and uncertainty evaluation of elemental and alloy liquids using electrostatic levitation", en, *Journal of Molecular Liquids* (2024), ISSN: 01677322, DOI: [10.1016/j.molliq.2024.123979](https://doi.org/10.1016/j.molliq.2024.123979).

[46] Paul-François Paradis, Takehiko Ishikawa, and Noriyuki Koike, "Thermophysical property measurements of liquid and supercooled cobalt.", *High Temperatures-High Pressures* (2008).

[47] Jonghyun Lee, Justin E. Rodriguez, Robert W. Hyers, and Douglas M. Matson, "Measurement of Density of Fe-Co Alloys Using Electrostatic Levitation", en, *Metallurgical and Materials Transactions B* (2015), ISSN: 1543-1916, DOI: [10.1007/s11663-015-0434-7](https://doi.org/10.1007/s11663-015-0434-7).

[48] Tunezō Saitō, Yutaka Shiraishi, and Yutaka Sakuma, “Density Measurement of Molten Metals by Levitation Technique at Temperatures between 1800° and 2200°C”, en, *Transactions of the Iron and Steel Institute of Japan* (1969), ISSN: 0021-1583, 1881-1183, DOI: [10.2355/isijinternational1966.9.118](https://doi.org/10.2355/isijinternational1966.9.118).

[49] X. J Han, N Wang, and B Wei, “Thermophysical properties of undercooled liquid cobalt”, en, *Philosophical Magazine Letters* (2002), ISSN: 0950-0839, 1362-3036, DOI: [10.1080/09500830210144382](https://doi.org/10.1080/09500830210144382).

[50] Jürgen Brillo, Ivan Egry, and Taishi Matsushita, “Density and excess volumes of liquid copper, cobalt, iron and their binary and ternary alloys”, en, *International Journal of Materials Research* (2006), ISSN: 2195-8556, 1862-5282, DOI: [10.3139/146.101415](https://doi.org/10.3139/146.101415).

[51] Manabu Watanabe, Junichi Takano, Masayoshi Adachi, Masahito Uchikoshi, and Hiroyuki Fukuyama, “Thermophysical properties of liquid Co measured by electromagnetic levitation technique in a static magnetic field”, en, *The Journal of Chemical Thermodynamics* (2018), ISSN: 00219614, DOI: [10.1016/j.jct.2018.02.004](https://doi.org/10.1016/j.jct.2018.02.004).

[52] Shunroku Watanabe, “Densities and Viscosities of Iron, Cobalt and Fe–Co Alloy in Liquid State”, en, *Transactions of the Japan Institute of Metals* (1971), ISSN: 0021-4434, 2432-4701, DOI: [10.2320/matertrans1960.12.17](https://doi.org/10.2320/matertrans1960.12.17).

[53] Kenneth C Mills, *Recommended values of thermophysical properties for selected commercial alloys*, Woodhead publishing, 2002, DOI: [10.1533/9781845690144](https://doi.org/10.1533/9781845690144).

[54] R. N. Abdullaev, R. A. Khairulin, Yu. M. Kozlovskii, and S. V. Stankus, “Density and Thermal Expansion of High Purity Cobalt over the Temperature Range from 140 K to 2073 K”, en, *Metallurgical and Materials Transactions A* (2021), ISSN: 1073-5623, 1543-1940, DOI: [10.1007/s11661-021-06485-1](https://doi.org/10.1007/s11661-021-06485-1).

[55] Marc J. Assael, Ivi J. Armyra, Juergen Brillo, Sergei V. Stankus, Jiangtao Wu, and William A. Wakeham, “Reference Data for the Density and Viscosity of Liquid Cadmium, Cobalt, Gallium, Indium, Mercury, Silicon, Thallium, and Zinc”, *Journal of Physical and Chemical Reference Data* (2012), ISSN: 0047-2689, DOI: [10.1063/1.4729873](https://doi.org/10.1063/1.4729873).

[56] LD Lucas, “SPECIFIC VOLUME OF MOLTEN METALS AND ALLOYS AT ELEVATED TEMPERATURES–PART 1”, *MEM SCI REV METALL* (1964).

[57] R.N. Abdullaev, R.A. Khairulin, Yu. M. Kozlovskii, A. Sh. Agazhanov, and S.V. Stankus, “Density of magnesium and magnesium-lithium alloys in solid and liquid states”, en, *Transactions of Nonferrous Metals Society of China* (2019), ISSN: 10036326, DOI: [10.1016/S1003-6326\(19\)64959-9](https://doi.org/10.1016/S1003-6326(19)64959-9).

[58] P. J. McGonigal, A. D. Kirshenbaum, and A. V. Grosse, “THE LIQUID TEMPERATURE RANGE, DENSITY, AND CRITICAL CONSTANTS OF MAGNESIUM¹”, en, *The Journal of Physical Chemistry* (1962), ISSN: 0022-3654, 1541-5740, DOI: [10.1021/j100810a038](https://doi.org/10.1021/j100810a038).

[59] Erich Gebhardt, Manfred Becker, and Erich Trägner, “Über die Eigenschaften metallischer Schmelzen: X. Die innere Reibung flüssiger Magnesium-Blei-Legierungen”, *International Journal of Materials Research* (1955), DOI: [10.1515/ijmr-1955-460204](https://doi.org/10.1515/ijmr-1955-460204).

[60] H. Grothe and C. Mangelsdorf, “The liquid temperature range, density, and critical constants of magnesium” (1937).

[61] S V Stankus and R A Khairulin, “Temperature and interphase changes in the density of magnesium in the solid and liquid states”, Russian, *Tsvetnye metally* (1990).

[62] K Arndt and G Ploetz, “The density of molten magnesium”, German, *Zeitschrift für Physikalische Chemie* (1927).

[63] JD Edwards and CS Taylor, “Density of magnesium from 20 to 700° C [J]”, *Transactions of the AIME* (1923).

[64] E Pelzel and F Sauerwald, “Density measurements at high temperatures XII”, *Zeitschrift für Metallkunde* (1941).

[65] Sangho Jeon, Shraddha Ganorkar, Yong Chan Cho, Joohyun Lee, Minju Kim, Jonghyun Lee, and Geun Woo Lee, “Precise density measurement and its uncertainty evaluation for refractory liquid metals over 3000 K using electrostatic levitation”, *Metrologia* (2022), ISSN: 0026-1394, 1681-7575, DOI: [10.1088/1681-7575/ac7688](https://doi.org/10.1088/1681-7575/ac7688).

[66] P.-F. Paradis, T. Ishikawa, and S. Yoda, “Noncontact Measurements of Thermophysical Properties of Molybdenum at High Temperatures”, *International Journal of Thermophysics* (2002), ISSN: 0195928X, DOI: [10.1023/A:1015169721771](https://doi.org/10.1023/A:1015169721771).

[67] BC Allen, “The surface tension of liquid transition metals at their melting points”, *Trans. AIME* (1963).

[68] John W Shaner, G Roger Gathers, and Camille Minichino, “Thermophysical properties of liquid tantalum and molybdenum”, *High Temperatures-High Pressures* (1977).

[69] U. Seydel and W. Kitzel, “Thermal volume expansion of liquid Ti, V, Mo, Pd, and W”, en, *Journal of Physics F: Metal Physics* (1979), ISSN: 0305-4608, DOI: [10.1088/0305-4608/9/9/001](https://doi.org/10.1088/0305-4608/9/9/001).

[70] D. V. Minakov, M. A. Paramonov, and P. R. Levashov, “Ab initio inspection of thermophysical experiments for molybdenum near melting”, *AIP Advances* (2018), ISSN: 2158-3226, DOI: [10.1063/1.5062152](https://doi.org/10.1063/1.5062152).

[71] R N Abdullaev, Yu M Kozlovskii, R A Khairulin, and S V Stankus, “Density and Thermal Expansion of High Purity Nickel over the Temperature Range from 150 K to 2030 K”, en, *Int J Thermophys* (2015), DOI: [10.1007/s10765-015-1839-x](https://doi.org/10.1007/s10765-015-1839-x).

[72] V.F. Ukhov, “Surface Properties and Density of the Palladium-Based Alloys”, PhD thesis, 1968.

[73] GD Ayushina, ES Levin, and PV Gel'd, “The density and surface energy of liquid alloys of aluminium with cobalt and nickel”, *Russ. J. Phys. Chem.* (1969).

[74] S. Y. Shiraishi and R. G. Ward, “The Density of Nickel in the Superheated and Supercooled Liquid States”, en, *Canadian Metallurgical Quarterly* (1964), ISSN: 0008-4433, 1879-1395, DOI: [10.1179/cmq.1964.3.1.117](https://doi.org/10.1179/cmq.1964.3.1.117).

[75] AD Kirshenbaum and J Cahill, "Densities of liquid nickel and cobalt and an estimate of their critical constants", *Trans. of ASM* (1963).

[76] LD Lucas, "Densite du fer, du nickel et du cobalt a l'etat liquid", *Comptes Rendus de l'Academie des Sciences* (1960).

[77] Tunezo SAITO and Yutaka SAKUMA, *Densities of Pure Iron, Cobalt and Nickel in the Molten State*, en, 1970, DOI: [10.50974/00042604](https://doi.org/10.50974/00042604).

[78] F.N. Tavadze, I.A. Bairamasvili, and D.V. Khantadze, Russian, *Surface Phenomena in Melts and in Solids Arising from the Melts*, Nalchik: Kabardino-Balkaria State University, 1965.

[79] L. Fang, F. Xiao, Y.F. Wang, Z.N. Tao, and K. MuKai, "Density and molar volume of liquid Ni-Co binary alloys", en, *Materials Science and Engineering: B* (2006), ISSN: 09215107, DOI: [10.1016/j.mseb.2006.02.015](https://doi.org/10.1016/j.mseb.2006.02.015).

[80] SI Popel, LM Shergin, and BV Tsarevskii, *TEMPERATURE VARIATION OF DENSITIES AND SURFACE TENSIONS OF IRON-NICKEL MELTS*, 1969.

[81] WD Drotning, "Thermal Expansion of Nickel to 2300 K", *Thermal Expansion 7*, Springer, 1982, DOI: [10.1007/978-1-4684-8267-6_2](https://doi.org/10.1007/978-1-4684-8267-6_2).

[82] LD Lucas and Mem Sci Rev Met, "Density of Metals at High Temperatures in the Solid and Molten States, Part 2", *Mem. Sci. Rev. Met* (1972).

[83] VN Eremenko and VI Nizhenko, "Surface Tension of Nickel Based Liquid Alloys. 1. The Ni-Sn-Al₂O₃ System", *Ukrainskii Khimicheskii Zhurnal* (1964).

[84] S V Stankus and R A Khairulin, "Thermophysics of Metastable Liquids in Relation with the Phenomena of Boiling and Crystallization", Russian, *Book of Abstracts, All-Union Symposium*, Sverdlovsk, 1985.

[85] Sang K. Chung, David B. Thiessen, and Won-Kyu Rhim, "A noncontact measurement technique for the density and thermal expansion coefficient of solid and liquid materials", en, *Review of Scientific Instruments* (1996), ISSN: 0034-6748, 1089-7623, DOI: [10.1063/1.1147584](https://doi.org/10.1063/1.1147584).

[86] Takehiko Ishikawa, Paul-Francois Paradis, and Yutaka Saita, "Thermophysical Property Measurements of Molten Nickel Using an Electrostatic Levitation Furnace", ja, *Journal of the Japan Institute of Metals* (2004), ISSN: 0021-4876, DOI: [10.2320/jinstmet.68.781](https://doi.org/10.2320/jinstmet.68.781).

[87] Hanbyeol Yoo, Cheolmin Park, Sangho Jeon, Soohyeong Lee, and Geun Woo Lee, "Uncertainty evaluation for density measurements of molten Ni, Zr, Nb and Hf by using a containerless method", *Metrologia* (2015), ISSN: 0026-1394, 1681-7575, DOI: [10.1088/0026-1394/52/5/677](https://doi.org/10.1088/0026-1394/52/5/677).

[88] Hidekazu Kobatake and Jürgen Brillo, "Density and thermal expansion of Cr-Fe, Fe-Ni, and Cr-Ni binary liquid alloys", en, *Journal of Materials Science* (2013), ISSN: 0022-2461, 1573-4803, DOI: [10.1007/s10853-013-7274-0](https://doi.org/10.1007/s10853-013-7274-0).

[89] J. Brillo, T. Schumacher, and K. Kajikawa, "Density of Liquid Ni-Ti and a New Optical Method for its Determination", en, *Metallurgical and Materials Transactions A* (2019), ISSN: 1073-5623, 1543-1940, DOI: [10.1007/s11661-018-5047-8](https://doi.org/10.1007/s11661-018-5047-8).

[90] Manabu Watanabe, Masayoshi Adachi, and Hiroyuki Fukuyama, "Densities of Fe-Ni melts and thermodynamic correlations", en, *Journal of Materials Science* (2016), ISSN: 0022-2461, 1573-4803, DOI: [10.1007/s10853-015-9644-2](https://doi.org/10.1007/s10853-015-9644-2).

[91] Shumpei Ozawa, Yu Kudo, Kazuhiko Kurabayashi, Yuki Watanabe, and Takehiko Ishikawa, "Precise density measurement of liquid titanium by electrostatic levitator", *Materials Transactions* (2017), DOI: [10.2320/matertrans.1-m2017835](https://doi.org/10.2320/matertrans.1-m2017835).

[92] Geun Woo Lee, Sangho Jeon, Cheolmin Park, and Dong-Hee Kang, "Crystal-liquid interfacial free energy and thermophysical properties of pure liquid Ti using electrostatic levitation: Hypercooling limit, specific heat, total hemispherical emissivity, density, and interfacial free energy", en, *The Journal of Chemical Thermodynamics* (2013), ISSN: 00219614, DOI: [10.1016/j.jct.2013.03.012](https://doi.org/10.1016/j.jct.2013.03.012).

[93] Takehiko Ishikawa and Paul-François Paradis, "Thermophysical properties of molten refractory metals measured by an electrostatic levitator", *Journal of electronic materials* (2005), DOI: [10.1007/s11664-005-0160-z](https://doi.org/10.1007/s11664-005-0160-z).

[94] Tunezo Saito, Yutaka Shiraishi, and Yutaka Sakuma, "Density measurement of molten metals by levitation technique at temperatures between 1800 and 2200 C", *Trans Iron Steel Inst Japan* (1969), DOI: [10.2355/isijinternational1966.9.118](https://doi.org/10.2355/isijinternational1966.9.118).

[95] Paul-François Paradis and Won-Kyu Rhim, "Non-contact measurements of thermophysical properties of titanium at high temperature", *The Journal of Chemical Thermodynamics* (2000), DOI: [10.1006/jcht.1999.0576](https://doi.org/10.1006/jcht.1999.0576).

[96] S. Jeon, D.-H. Kang, Y. H. Lee, S. Lee, and G. W. Lee, "Effect of atomic size on undercoolability of binary solid solution alloy liquids with Zr, Ti, and Hf using electrostatic levitation", en, *The Journal of Chemical Physics* (2016), ISSN: 0021-9606, 1089-7690, DOI: [10.1063/1.4966649](https://doi.org/10.1063/1.4966649).

[97] S. Amore, S. Delsante, H. Kobatake, and J. Brillo, "Excess volume and heat of mixing in Cu-Ti liquid mixture", en, *The Journal of Chemical Physics* (2013), ISSN: 0021-9606, 1089-7690, DOI: [10.1063/1.4817679](https://doi.org/10.1063/1.4817679).

[98] Manabu Watanabe, Masayoshi Adachi, and Hiroyuki Fukuyama, "Density measurement of Ti-X (X = Cu, Ni) melts and thermodynamic correlations", en, *Journal of Materials Science* (2019), ISSN: 0022-2461, 1573-4803, DOI: [10.1007/s10853-018-3098-2](https://doi.org/10.1007/s10853-018-3098-2).

[99] M Leitner and G Pottlacher, "Density of liquid niobium and tungsten and the estimation of critical point data", *Metallurgical and Materials Transactions A* (2019), DOI: [10.1007/s11661-019-05262-5](https://doi.org/10.1007/s11661-019-05262-5).

[100] SV Koval', NI Kuskova, and SI Tkachenko, "Investigation of the mechanism of electric explosion of conductors and of the thermal characteristics of liquid metals", *Teplofizika vysokikh temperatur* (1997).

[101] H Hess, A Kloss, A Rakhel, and H Schneidenbach, "Determination of thermophysical properties of fluid metals by wire-explosion experiments", *International journal of thermophysics* (1999), DOI: [10.1023/a:1022635727340](https://doi.org/10.1023/a:1022635727340).

[102] T Hüpf, C Cagran, G Lohöfer, and G Pottlacher, “Electrical resistivity of high melting metals up into the liquid phase (V, Nb, Ta, Mo, W)”, en, *Journal of Physics: Conference Series* (2008), ISSN: 1742-6588, 1742-6596, DOI: [10.1088/1742-6596/98/6/062002](https://doi.org/10.1088/1742-6596/98/6/062002).

[103] RS Hixson and MA Winkler, “Thermophysical properties of solid and liquid tungsten”, *International Journal of Thermophysics* (1990), DOI: [10.1007/bf01184339](https://doi.org/10.1007/bf01184339).

[104] A Berthault, L Arles, and J Matricon, “High-pressure, high-temperature thermophysical measurements on tantalum and tungsten”, *International journal of thermophysics* (1986), DOI: [10.1007/bf00503808](https://doi.org/10.1007/bf00503808).

[105] A Calverley, “A determination of the surface tension of liquid tungsten by the drop-weight method”, *Proceedings of the Physical Society. Section B* (1957), DOI: [10.1088/0370-1301/70/11/303](https://doi.org/10.1088/0370-1301/70/11/303).

[106] A. Meyer, S. Stüber, D. Holland-Moritz, O. Heinen, and T. Unruh, “Determination of self-diffusion coefficients by quasielastic neutron scattering measurements of levitated Ni droplets”, en, *Physical Review B* (2008), ISSN: 1098-0121, 1550-235X, DOI: [10.1103/PhysRevB.77.092201](https://doi.org/10.1103/PhysRevB.77.092201).

[107] F Kargl, H Weis, T Unruh, and A Meyer, “Self diffusion in liquid aluminium”, en, *Journal of Physics: Conference Series* (2012), ISSN: 1742-6588, 1742-6596, DOI: [10.1088/1742-6596/340/1/012077](https://doi.org/10.1088/1742-6596/340/1/012077).

[108] F. Demmel, D. Szubrin, W.-C. Pilgrim, and C. Morkel, “Diffusion in liquid aluminium probed by quasielastic neutron scattering”, en, *Physical Review B* (2011), ISSN: 1098-0121, 1550-235X, DOI: [10.1103/PhysRevB.84.014307](https://doi.org/10.1103/PhysRevB.84.014307).

[109] J. Horbach, R. E. Rozas, T. Unruh, and A. Meyer, “Improvement of computer simulation models for metallic melts via quasielastic neutron scattering: A case study of liquid titanium”, en, *Physical Review B* (2009), ISSN: 1098-0121, 1550-235X, DOI: [10.1103/PhysRevB.80.212203](https://doi.org/10.1103/PhysRevB.80.212203).

[110] H Okamoto, M E Schlesinger, and E M Mueller, eds., *Alloy Phase Diagrams*, ASM International, 2016, DOI: [10.31399/asm.hb.v03.9781627081634](https://doi.org/10.31399/asm.hb.v03.9781627081634).

[111] Kurt Lejaeghere, Veronique Van Speybroeck, Guido Van Oost, and Stefaan Cottenier, “Error estimates for solid-state density-functional theory predictions: an overview by means of the ground-state elemental crystals”, *Critical reviews in solid state and materials sciences* (2014), DOI: [10.1080/10408436.2013.772503](https://doi.org/10.1080/10408436.2013.772503).

[112] Yunsheng Liu, Xingfeng He, and Yifei Mo, “Discrepancies and error evaluation metrics for machine learning interatomic potentials”, en, *npj Computational Materials* (2023), Number: 1 Publisher: Nature Publishing Group, ISSN: 2057-3960, DOI: [10.1038/s41524-023-01123-3](https://doi.org/10.1038/s41524-023-01123-3).

[113] I. A. Balyakin, S. V. Rempel, R. E. Ryltsev, and A. A. Rempel, “Deep machine learning interatomic potential for liquid silica”, *Physical Review E* (2020), Publisher: American Physical Society, DOI: [10.1103/PhysRevE.102.052125](https://doi.org/10.1103/PhysRevE.102.052125).

[114] Fang Fang, Jie Lin, Jiajia Li, Yu Zhang, Qiuyi Fu, Quanquan Zhou, Wei Li, Guobing Zhou, and Zhen Yang, “Molecular dynamics simulations of liquid gallium alloy Ga-X (X = Pt, Pd, Rh) via machine learning potentials”, en, *Inorganic Chemistry Frontiers* (2024), Publisher: Royal Society of Chemistry, DOI: [10.1039/D3QI02410E](https://doi.org/10.1039/D3QI02410E).

[115] Claudio Zeni, Kevin Rossi, Theodore Pavloudis, Joseph Kioseoglou, Stefano de Gironcoli, Richard E. Palmer, and Francesca Baletto, “Data-driven simulation and characterisation of gold nanoparticle melting”, en, *Nature Communications* (2021), Publisher: Nature Publishing Group, ISSN: 2041-1723, DOI: [10.1038/s41467-021-26199-7](https://doi.org/10.1038/s41467-021-26199-7).

[116] Cameron J. Owen, Steven B. Torrisi, Yu Xie, Simon Batzner, Kyle Bystrom, Jennifer Coulter, Albert Musaelian, Lixin Sun, and Boris Kozinsky, *Complexity of Many-Body Interactions in Transition Metals via Machine-Learned Force Fields from the TM23 Data Set*, arXiv:2302.12993 [cond-mat, physics:physics], 2023, DOI: [10.48550/arXiv.2302.12993](https://doi.org/10.48550/arXiv.2302.12993).

[117] Ganesh Sivaraman, Anand Narayanan Krishnamoorthy, Matthias Baur, Christian Holm, Marius Stan, Gábor Csányi, Chris Benmore, and Álvaro Vázquez-Mayagoitia, “Machine-learned interatomic potentials by active learning: amorphous and liquid hafnium dioxide”, en, *npj Computational Materials* (2020), Publisher: Nature Publishing Group, ISSN: 2057-3960, DOI: [10.1038/s41524-020-00367-7](https://doi.org/10.1038/s41524-020-00367-7).

[118] Yunxing Zuo, Chi Chen, Xiangguo Li, Zhi Deng, Yiming Chen, Jörg Behler, Gábor Csányi, Alexander V. Shapeev, Aidan P. Thompson, Mitchell A. Wood, and Shyue Ping Ong, “Performance and Cost Assessment of Machine Learning Interatomic Potentials”, *The Journal of Physical Chemistry A* (2020), Publisher: American Chemical Society, ISSN: 1089-5639, DOI: [10.1021/acs.jpca.9b08723](https://doi.org/10.1021/acs.jpca.9b08723).

[119] Killian Sheriff, Daniel Xiao, Yifan Cao, Lewis R Owen, and Rodrigo Freitas, “Machine learning potentials for modeling alloys across compositions”, *arXiv preprint arXiv:2506.12592* (2025), DOI: [10.48550/arXiv.2506.12592](https://doi.org/10.48550/arXiv.2506.12592).

[120] Georg Kresse and Daniel Joubert, “From ultrasoft pseudopotentials to the projector augmented-wave method”, *Physical review b* (1999).

[121] G Kresse and J Hafner, “Ab initio molecular dynamics for liquid metals”, en, *Phys. Rev. B Condens. Matter* (1993), DOI: [10.1103/PhysRevB.47.558](https://doi.org/10.1103/PhysRevB.47.558).

[122] G Kresse and J Furthmüller, “Efficient iterative schemes for ab initio total-energy calculations using a plane-wave basis set”, en, *Phys. Rev. B Condens. Matter* (1996), DOI: [10.1103/PhysRevB.54.11169](https://doi.org/10.1103/PhysRevB.54.11169).

[123] G Kresse and J Furthmüller, “Efficiency of ab-initio total energy calculations for metals and semiconductors using a plane-wave basis set”, en, *Comput. Mater. Sci.* (1996), DOI: [10.1016/0927-0256\(96\)00008-0](https://doi.org/10.1016/0927-0256(96)00008-0).

[124] G Kresse and J Hafner, “Ab initio molecular-dynamics simulation of the liquid-metal-amorphous-semiconductor transition in germanium”, en, *Phys. Rev. B Condens. Matter* (1994), DOI: [10.1103/PhysRevB.49.14251](https://doi.org/10.1103/PhysRevB.49.14251).

[125] Peter E Blochl et al., “Projector augmented-wave method”, *Phys. rev. B* (1994).

[126] Pandu Wisesa, Kyle A McGill, and Tim Mueller, “Efficient generation of generalized Monkhorst-Pack grids through the use of informatics”, *Physical Review B* (2016), DOI: [10.1103/physrevb.93.155109](https://doi.org/10.1103/physrevb.93.155109).

[127] Yunzhe Wang, Pandu Wisesa, Adarsh Balasubramanian, Shyam Dwaraknath, and Tim Mueller, “Rapid generation of optimal generalized Monkhorst-Pack grids”, *Computational Materials Science* (2021), DOI: [10.1016/j.commatsci.2020.110100](https://doi.org/10.1016/j.commatsci.2020.110100).

[128] Anton Bochkarev, Yury Lysogorskiy, Sarath Menon, Mi-naam Qamar, Matous Mrovec, and Ralf Drautz, “Efficient parametrization of the atomic cluster expansion”, *Physical Review Materials* (2022), Publisher: American Physical Society, DOI: [10.1103/PhysRevMaterials.6.013804](https://doi.org/10.1103/PhysRevMaterials.6.013804).

[129] James F Ziegler, Jochen P Biersack, and Uffe Littmark, *The Stopping and Range of Ions in Solids*, New York: Pergamon Press, 1985.

[130] Aidan P. Thompson, H. Metin Aktulga, Richard Berger, Dan S. Bolintineanu, W. Michael Brown, Paul S. Crozier, Pieter J. in 't Veld, Axel Kohlmeyer, Stan G. Moore, Trung Dac Nguyen, Ray Shan, Mark J. Stevens, Julien Tranchida, Christian Trott, and Steven J. Plimpton, “LAMMPS - a flexible simulation tool for particle-based materials modeling at the atomic, meso, and continuum scales”, *Computer Physics Communications* (2022), ISSN: 0010-4655, DOI: [10.1016/j.cpc.2021.108171](https://doi.org/10.1016/j.cpc.2021.108171).

[131] Glenn J Martyna, Douglas J Tobias, and Michael L Klein, “Constant pressure molecular dynamics algorithms”, *J. chem. Phys* (1994), DOI: [10.1063/1.467468](https://doi.org/10.1063/1.467468).

[132] Mark E Tuckerman, José Alejandre, Roberto López-Rendón, Andrea L Jochim, and Glenn J Martyna, “A Liouville-operator derived measure-preserving integrator for molecular dynamics simulations in the isothermal–isobaric ensemble”, *Journal of Physics A: Mathematical and General* (2006), DOI: [10.1088/0305-4470/39/19/S18](https://doi.org/10.1088/0305-4470/39/19/S18).

[133] Wataru Shinoda, Motoyuki Shiga, and Masuhiro Mikami, “Rapid estimation of elastic constants by molecular dynamics simulation under constant stress”, *Physical Review B* (2004), DOI: [10.1103/PhysRevB.69.134103](https://doi.org/10.1103/PhysRevB.69.134103).

[134] Michele Parrinello and Aneesur Rahman, “Polymorphic transitions in single crystals: A new molecular dynamics method”, *Journal of Applied physics* (1981), DOI: [10.1063/1.328693](https://doi.org/10.1063/1.328693).

[135] Christopher Jarzynski, “Nonequilibrium equality for free energy differences”, *Physical Review Letters* (1997), DOI: [10.1103/physrevlett.78.2690](https://doi.org/10.1103/physrevlett.78.2690).

[136] Harald Oberhofer, Christoph Dellago, and Phillip L Geissler, “Biased sampling of nonequilibrium trajectories: Can fast switching simulations outperform conventional free energy calculation methods?”, *The Journal of Physical Chemistry B* (2005), DOI: [10.1021/jp044556a](https://doi.org/10.1021/jp044556a).

[137] Rodrigo Freitas, Mark Asta, and Maurice De Koning, “Nonequilibrium free-energy calculation of solids using LAMMPS”, *Computational Materials Science* (2016), DOI: [10.1016/j.commatsci.2015.10.050](https://doi.org/10.1016/j.commatsci.2015.10.050).

[138] Maurice de Koning, A Antonelli, and Sidney Yip, “Optimized free-energy evaluation using a single reversible-scaling simulation”, *Physical review letters* (1999), DOI: [10.1103/physrevlett.83.3973](https://doi.org/10.1103/physrevlett.83.3973).

[139] Daan Frenkel and Anthony J. C. Ladd, “New Monte Carlo method to compute the free energy of arbitrary solids. Application to the fcc and hcp phases of hard spheres”, *The Journal of Chemical Physics* (1984), ISSN: 0021-9606, DOI: [10.1063/1.448024](https://doi.org/10.1063/1.448024).

[140] Rodolfo Paula Leite, Pedro Antonio Santos-Flórez, and Maurice de Koning, “Uhlenbeck-Ford model: Phase diagram and corresponding-states analysis”, *Physical Review E* (2017), DOI: [10.1103/physreve.96.032115](https://doi.org/10.1103/physreve.96.032115).

[141] Rodolfo Paula Leite and Maurice de Koning, “Nonequilibrium free-energy calculations of fluids using LAMMPS”, *Computational Materials Science* (2019), DOI: [10.1016/j.commatsci.2018.12.029](https://doi.org/10.1016/j.commatsci.2018.12.029).

[142] Rodolfo Paula Leite, Rodrigo Freitas, Rodolfo Azevedo, and Maurice de Koning, “The Uhlenbeck-Ford model: Exact virial coefficients and application as a reference system in fluid-phase free-energy calculations”, *The Journal of chemical physics* (2016), DOI: [10.1063/1.4967775](https://doi.org/10.1063/1.4967775).